Biochimica et Biophysica Acta 1788 (2009) 743–752

Contents lists available at ScienceDirect

Biochimica et Biophysica Acta

journal homepage: www.elsevier.com/locate/bbamem

# Mechanistic role of ergosterol in membrane rigidity and cycloheximide resistance in *Saccharomyces cerevisiae*

Fumiyoshi Abe *, Toshiki Hiraki

*Extremobiosphere Research Center, Japan Agency for Marine-Earth Science and Technology (JAMSTEC), 2-15 Natsushima-cho, Yokosuka 237-0061, Japan*

ARTICLE INFO

*Article history:*
Received 10 October 2008
Received in revised form 19 November 2008
Accepted 3 December 2008
Available online 11 December 2008

*Keywords:*
Ergosterol
TMA-DPH
Fluorescence anisotropy
Membrane rigidity and fluidity
Drug permeability

ABSTRACT

Mutants of *Saccharomyces cerevisiae* defective in the late steps of ergosterol biosynthesis are viable but accumulate structurally altered sterols within the plasma membrane. Despite the significance of pleiotropic abnormalities in the *erg* mutants, little is known about how sterol alterations mechanically affect the membrane structure and correlate with individual mutant phenotypes. Here we demonstrate that the membrane order and occurrence of voids are determinants of membrane rigidity and hypersensitivity to a drug. Among five *erg*Δ mutants, the *erg2*Δ mutant exhibited the most marked sensitivity to cycloheximide. Notably, measurement of time-resolved anisotropy indicated that the *erg2*Δ mutation decreased the membrane order parameter ($S$), and dramatically increased the rotational diffusion coefficient ($D_w$) of 1-[4-(trimethylamino)pheny]-6-phenyl-1,3,5-hexatriene (TMA-DPH) in the plasma membrane by 8-fold, providing evidence for the requirement of ergosterol for membrane integrity. The $IC_{50}$ of cycloheximide was closely correlated with $S/D_w$ in these strains, suggesting that the membrane disorder and increasing occurrence of voids within the plasma membrane synergistically enhance passive diffusion of cycloheximide across the membrane. Exogenous ergosterol partially restored the membrane properties in the *upc2-1erg2*Δ strain. In this study, we describe the ability of ergosterol to adjust the dynamic properties of the plasma membrane, and consider the relevance of drug permeability.



## 1. Introduction

The eukaryotic plasma membrane is a complex structure consisting of thousands of different lipids with numerous embedded membrane proteins. Experimental evidence from a variety of studies indicated the heterogeneity of lateral organization of the plasma membrane lipids [1]. The emerging concept of floating entities in the plasma membrane known as “rafts” has received a great deal of attention because rafts are believed to be involved in cellular regulation and functions such as signal transduction, endocytosis, membrane trafficking and in pathogenesis [2–5]. The widely used operational description of rafts is based on the fractionation of detergent-resistant membranes (DRMs) obtained by the extraction of living cell membranes with cold nonionic detergents. DRMs in the yeast *Saccharomyces cerevisiae* are enriched in ergosterol, sphingolipids, and a variety of specific membrane proteins [6]. Despite the lack of clarification of the role of lipid rafts in yeast, ergosterol plays an essential role in bulk membrane function, affecting membrane rigidity, fluidity, and permeability [7]. Many of the most successful antifungal agents in the medical and agrochemical fields interfere with sterol biosynthesis or function [8], and thus drug permeability of the plasma membrane is one of the major targets of pharmaceutical development. In *S. cerevisiae*, genes encoding proteins that catalyze the final five steps in ergosterol biosynthesis are nonessential, and the viable ergosterol (*erg*) mutants accumulate altered sterols that are structurally distinct from ergosterol [9,10]. The changes in sterol composition caused by *erg* mutations confer pleiotropic hypersensitivity to a broad range of compounds such as LiCl, NaCl, ethanol, cycloheximide, anthracyclines, dactinomycin, and brefeldin A [11–15]. The viability of *erg* mutants enables us to analyze whether specific structural ergosterol motifs are required for specific cellular processes. The hypersensitivity of the *erg6*Δ mutant to cycloheximide has been accounted for by two distinct mechanisms [15,16]. First, the membrane bilayer of the *erg6*Δ mutant is permeable to small molecules. Second, sterol alteration in the *erg6*Δ mutant decreases the activity of a multidrug efflux pump, Pdr5, and thereby cycloheximide is accumulated in the *erg6*Δ cells. The results of Emter et al. supported the first mechanism showing that Pdr5 was functional in the *erg6*Δ mutant and that deletions for *ERG6* and *PDR5* enhanced drug accumulation in an additive fashion [15].

*Abbreviations:* DPH, 1,6-diphenyl-1,3,5-hexatriene; TMA-DPH, 1-[4-(trimethylamino)pheny]-6-phenyl-1,3,5-hexatriene; TCSPC, time-correlated single-photon counting; DMPC, 1,2-dimyristoyl-*sn*-glycero-3-phosphocholine; $r_s$, steady-state anisotropy; $r_0$, maximum anisotropy; $r_\infty$, limiting anisotropy; $\theta$, rotational correlation time; $S$, order parameter; $D_w$, rotational diffusion coefficient

* Corresponding author. Tel.: +81 46 867 9678; fax: +81 46 867 9715.
*E-mail address:* abef@jamstec.go.jp (F. Abe).

0005-2736/$ – see front matter © 2008 Elsevier B.V. All rights reserved.
doi:10.1016/j.bbamem.2008.12.002

Specific sterols are required for receptor-mediated endocytosis, fluid-phase endocytosis [17–19], and trafficking of the tryptophan permease Tat2 [20,21]. *ELO3* encodes a protein required to produce a very long-chain fatty acid (C26) in sphingolipids and is synthetically lethal with mutations in *ERG6* [22]. In a conditional *elo3Δerg6*$^{ts}$ double-mutant, the plasma membrane $H^+$-ATPase Pma1 fails to associate with rafts and is rerouted to the vacuole for degradation [22]. Ergosterol is also required for actin cytoskeletal organization when the endosomal protein complex Cdc50-Drs2 is lost [23]. In yeast mating, ergosterol depletion inhibits pheromone signaling and plasma membrane fusion [24]. Accordingly, ergosterol is clearly important for membrane integrity and diverse cellular functions in yeast. Nevertheless, little attention has been paid to how sterol alterations mechanically correlate with membrane properties. High hydrostatic pressure packs lipid bilayers and low temperature reduces the thermal motion of the acyl chains, and thereby act toward ordering the membranes. In our genome-wide functional screening using a yeast deletion library, we found that ergosterol was required for growth under high pressure of 25 MPa (approximately 250 kg/cm$^2$) and low temperature of 15 °C [25]. This implies that ergosterol but not altered sterols allows the plasma membrane and/or membrane proteins to fulfill functions when the membrane is highly ordered. However, no theory has been proposed to describe the phenotypic abnormalities of the five *erg* mutants consistent with changes in membrane properties.

The role played by lipid molecules in the function and structure of biological membranes has been widely analyzed using a variety of physical techniques. Fluorescence depolarization techniques are particularly suitable for this purpose. Two lipophilic molecules, 1,6-diphenyl-1,3,5-hexatriene (DPH) and 1-[4-(trimethylamino)pheny]-6-phenyl-1,3,5-hexatriene (TMA-DPH), are commonly utilized in such experiments [26–28]. Measurement of the steady-state anisotropy of DPH is the most common technique to estimate macroscopic membrane rigidity. Importantly, it evaluates equally fluid and less-fluid regions of the membrane [29]. In model lipid membranes, cholesterol and ergosterol are generally thought to have packing effects on bilayer acyl chains in the liquid-crystalline phase and disordering effects in the gel phase [30,31]. However, in intact mammalian cells, a major problem in using DPH is that the dye accumulates both in the plasma membrane and organelle membranes, thus characterizing the total membrane apparatus rather than the plasma membrane alone [32]. In *S. cerevisiae*, Parks and colleagues performed anisotropy measurement with purified plasma membrane and showed that membrane rigidity was lost in sterol auxotrophs [33]. However, it has been established that DPH exhibits a bimodal orientational distribution, i.e., perpendicular to the bilayer plane near the center of the membrane and parallel to it within the acyl-chain tails, making interpretation complex [34]. TMA-DPH is a derivative of DPH. Due to its cationic moiety, it is anchored with the charged headgroup at the lipid–water interface and thereby reflects only the interfacial region of the membrane [27]. In mammalian cells, it remains localized randomly in the plasma membrane [32]. It was reported that the *erg* mutants lost rigidity of the plasma membrane [35]. However, steady-state anisotropy is insufficient to describe precisely the dynamic membrane properties because they are a function of various parameters such as probe motion, fluorescence lifetime, lipid composition, and hydration.

Time-resolved fluorescence spectroscopy based on time-correlated single-photon counting (TCSPC) enables us to determine the principal parameters such as the rotational correlation time, membrane order parameter, limiting anisotropy, and fluorescence lifetime in a single measurement [28]. Additionally, the possibility of characterizing membrane heterogeneity using this technique could be important to improve our knowledge of membrane structure and dynamics and their physiologic implications. Nevertheless, this technique has not been extensively employed in yeast cell biology.

To elucidate the mechanistic role of ergosterol in membrane properties, we introduced this optical technique into the investigation of ergosterol biosynthetic mutants in an attempt to determine the relevance of that role based on the physiologic traits of yeast. In this study, we demonstrate important parameters that characterize the dynamics of the plasma membrane of five *erg* mutants and indicate a link to cycloheximide susceptibility.

## 2. Materials and methods

### 2.1. Yeast strains and culture conditions

The wild-type strains BY4742 (*MAT*α *his3Δ1 leu2Δ0 lys2Δ0 ura3Δ0*) and BY4741 (*MAT*a *his3Δ1 leu2Δ0 lys2Δ0 ura3Δ0*), and the *erg2Δ::kanMX4*, *erg3Δ::kanMX4*, *erg4Δ::kanMX4*, *erg5Δ::kanMX4*, *erg6Δ::kanMX4*, and *pdr5Δ::kanMX4* mutants were obtained from the EUROSCARF yeast-deletion library (cat. no. 95400.H3, Invitrogen, Carlsbad, CA, USA) [36]. Strain WPY361 (*MAT*a *upc2-1 ura3-1 his3-11, -15 leu2-3,-112 trp1-1*) was kindly provided by W.A. Prinz of the US National Institutes of Health (Bethesda, MD, USA) [37]. Cells were grown in synthetic complete (SC) medium with slight modification [38] with vigorous shaking at 25 °C. The optical density at 600 nm ($OD_{600}$) was measured after appropriate dilution of the samples. Cycloheximide, rhodamine 6G, ergosterol (Wako Pure Chemical Industries Inc., Osaka, Japan), and Tween 80 (Sigma-Aldrich Inc., St. Louis, MO, USA) were used as additives in the growth medium. Ergosterol was dissolved in Tween 80-ethanol solution to give a stock solution of 50 mM as described previously [37].

### 2.2. Cycloheximide sensitivity

Exponentially growing cells were diluted in SC medium at 0.001 $OD_{600}$, and the cells were exposed to various concentrations of cycloheximide in 96-well plates at 25 °C for 48 h. The $OD_{600}$ was measured using an MTP-450 plate leader (Corona Electric Co., Ltd., Hitachinaka, Japan).

### 2.3. Genetic manipulation

To confer tryptophan prototrophy on strain WPY361, an EcoRI–SphI fragment from plasmid pJJ280 containing *TRP1* was introduced into the cells, giving strain FAS421 (*MAT*a *upc2-1 ura3-1 his3-11,-15 leu2-3,-112*). To create the *erg2Δ::kanMX4* mutation in strain FAS421, PCR-based gene disruption was carried out using the primers ERG2a (ATCGAACCACGGCCCTCGTATAAGCCGC) and ERG2b (CACCGCTTT-CAAAGAATTGAAGATTGAG) and genomic DNA purified from the *erg2Δ::kanMX4* mutant as a template, giving strain FAS415 (*MAT*a *erg2Δ::kanMX4 upc2-1 ura3-1 his3-11,-15 leu2-3,-112*). Deletion of *ERG2* was confirmed by PCR amplification of the genomic DNA using the primers ERG2a700 (TAACTGCGAGAGGCCGGGTTTTTAAAGG) and kanC-b (ATTACGCTCGTCATCAAAATCA).

### 2.4. Labeling of cells with DPH and TMA-DPH

Cells were grown in SC medium at 25 °C at 0.5–1.0 $OD_{600}$ (~0.5–1.0×10$^7$ cells ml$^{-1}$). The cells were collected by centrifugation, washed twice with TE buffer (10 mM Tris–Cl, 1 mM EDTA, pH 7.0) and labeled with DPH or TMA-DPH (Invitrogen) at 25 °C for 10 min in the dark. Unless otherwise specified, DPH and TMA-DPH were used at concentrations of 5.0 μM and 0.5 μM, respectively. After washing twice, the cells were resuspended in TE buffer at 0.25 $OD_{600}$ and placed on ice until use. The cell suspensions were warmed at 25 °C for 4 min prior to subsequent measurements. The leakage of fluorescent dyes from the labeled cells was negligible during the storage on ice, prewarming, and anisotropy measurements judging from the fluorescence intensity of labeled cells.

### 2.5. Preparation of DMPC vesicles

1,2-Dimyristoyl-*sn*-glycero-3-phosphocholine (DMPC; Wako Pure Chemical Industries Inc.) was dissolved in chloroform, and the solvent was removed under a vacuum for 10 min. It was suspended in TE buffer at a concentration of 200 μM with a vortex and sonication. The membranes were allowed to swell in TE buffer at 30 °C for 1 h and subsequently labeled with 0.5 μM TMA-DPH at 30 °C for 1 h in the dark.

### 2.6. Steady-state anisotropy measurement

An RF-5300PC spectrofluorometer with a xenon arc lamp and polarizing device (Shimadzu Co., Kyoto, Japan) was used for the measurement of the steady-state anisotropy of TMA-DPH. The excitation and emission wavelengths were 358 nm and 430 nm, respectively. The measurement was carried out at 25 °C. To avoid photobleaching of the dye, labeled cells were excited for 0.25 s. The steady-state anisotropy ($r_s$) was calculated from polarized intensities according to the equation:

$$r_s = (I_{VV} - G I_{VH})/(I_{VV} + 2G I_{VH}) \quad (1)$$

where $I$ is the fluorescence intensity of TMA-DPH-labeled cells after subtraction of that of unlabeled cells. The subscript VV indicates measurements with both polarizers positioned vertically, while the subscript VH indicates measurements with the excitation polarizer in the vertical and the emission polarizer in the horizontal position. $G$ stands for the $G$-factor, $I_{HV}/I_{HH}$, for this instrument. The subscripts HV and HH indicate the positions of polarizers opposite VH and VV, respectively. Data are expressed as means with standard deviations from more than three independent experiments.

### 2.7. Time-resolved fluorescence spectroscopy

A FluoroCube (Horiba Ltd., Kyoto, Japan) capable of performing TCSPC was used for the measurement of time-resolved fluorescence anisotropy of TMA-DPH. The instrument was equipped with a polarizing device and a 375-nm laser diode (NanoLED 375 L, Horiba Ltd.) operated with a pulse frequency of 1 MHz. Because the laser power is extremely low (6–7 μW), photobleaching of the dye is negligible. TMA-DPH-labeled cells were placed in a quartz cuvette at 0.4 $OD_{600}$. Fluorescence was emitted at 460 nm at 25 °C. The time ($t$) axis ranging from 0 to 228 ns was split into 2048 channels. $I_{VH}(t)$ and $I_{VV}(t)$ were measured sequentially in cycles between $I_{VH}(t)$ and $I_{VV}(t)$. The $G$-factor was determined by measuring $I_{HH}(t)$ and $I_{HV}(t)$ for 1 min each. The instrumental response function was obtained by measuring the Rayleigh scattering light from the cell samples at 375 nm. Parameters describing the fluorescence intensity decay and anisotropy decay were determined by convolving $I_{VH}(t)$ and $I_{VV}(t)$ and the instrument response function. Data were analyzed using the DAS6 decay analysis software, version 6.3 (Horiba Ltd.). The simplest model of the restricted motion of fluorochromes in the membrane, based on the Brownian diffusion of the label in a cone with a wobbling diffusion constant, leads to the following single exponential approximation of the anisotropy decay with time, $r(t)$ [26]:

$$r(t) = (r_0 - r_\infty)\cdot\exp(-t/\theta) + r_\infty \quad (2)$$

where $r_0$ stands for the maximum anisotropy, $r_\infty$ for limiting anisotropy, and $\theta$ (ns) for rotational correlation time. The order parameter ($S$) is calculated to obtain the structural information on the membrane according to the following equation:

$$S = (r_\infty/r_0)^{1/2} \quad (3)$$

The rotational (wobbling) diffusion coefficient ($D_w$) was calculated to obtain the dynamic nature of the membrane according to the following equation:

$$D_w = (r_0 - r_\infty)/6\theta r_0 \quad (4)$$

### 2.8. Fluorescence microscopy

An FV500 confocal laser microscope equipped with a 405-nm UV laser (Olympus Corporation, Tokyo, Japan) was used to visualize DPH and TMA-DPH labeling of the cells.

### 2.9. Estimation of free sterol levels

Free sterol contents in crude membrane extracts were preliminarily estimated using a kit. A P13 membrane fraction was prepared as described previously with slight modification [38]. Briefly, $4\times10^8$ cells were collected by centrifugation and washed twice with TE buffer. The cells were broken with glass beads. Unbroken cells and debris were removed by centrifugation at 500 ×*g* for 2 min. The whole-cell extract was centrifuged at 13,000 ×*g* for 10 min to collect the P13 membrane fraction. The resulting P13 membrane was suspended in 104 μl of water. Four microliters of the membrane fraction was subjected to determination of total protein contents using a Bio-Rad Protein Assay (Bio-Rad Laboratories, Inc., Hercules, CA, USA). The remaining solution was mixed with an equal volume of 20% Triton X-100 (SigmaUltra, Sigma-Aldrich Inc.), and the mixture was kept at 25 °C for 30 min to solubilize the membranes. Fifty microliters of the membrane solution was subjected to the detection of free sterols using a kit (Free cholesterol E-test, Wako Pure Chemical Industries, Inc.) based on the enzymatic detection of hydrogen peroxide generated from oxidizing free sterols with cholesterol oxidase. In our estimation, cholesterol oxidase in the kit catalyzed ergosterol (ergosterol standard, purity >98%, Wako Pure Chemical Industries Inc.) at an efficiency of 78 ± 12% ($n$=3) to the cholesterol standard substrate provided in the kit, allowing us to estimate free sterol levels in the P13 membrane fractions. The catalytic efficiency for various structurally altered sterols in the *erg* mutants remains to be defined, and thus we provide data as preliminary results.

## 3. Results

### 3.1. *erg*Δ mutants exhibit varying cycloheximide sensitivity

Fig. 1A illustrates the final five steps in ergosterol biosynthesis catalyzed by Erg proteins. We examined whether cycloheximide sensitivity had been conferred on the five viable *erg*Δ mutants isogenic to strain BY4742. A known drug-sensitive mutant, *pdr5*Δ, was used as a reference [15,16]. Consistent with previous reports [15,16], most viable *erg*Δ mutants exhibited hypersensitivity to cycloheximide, except for the *erg*5Δ mutant that exhibited greater resistance than the wild-type strain (Fig. 2A). The *erg*5Δ mutant has not previously been examined for cycloheximide sensitivity. The *erg2*Δ mutant exhibited the most marked sensitivity. The order of cycloheximide resistance was *erg2*Δ < *erg6*Δ < *erg3*Δ, *erg4*Δ < *pdr5*Δ < wild-type < *erg5*Δ. Structures of ergosterol and altered sterols accumulated in the *erg2*Δ mutant [18] are shown in Fig. 1B and C. Heterozygous diploids formed with *erg*Δ mutants and the wild-type strain BY4741 exhibited cycloheximide resistance similar to the homozygous wild-type diploid strain, indicating that the mutant phenotype is recessive (Fig. 2B). The hypersensitivity to cycloheximide is likely attributable to enhanced passive diffusion of this lipophilic compound across the plasma membrane when the sterol composition is altered. The *erg6*Δ mutation is known to enhance passive diffusion of rhodamine 6G across the plasma membrane [15]. Consistent with this, we have

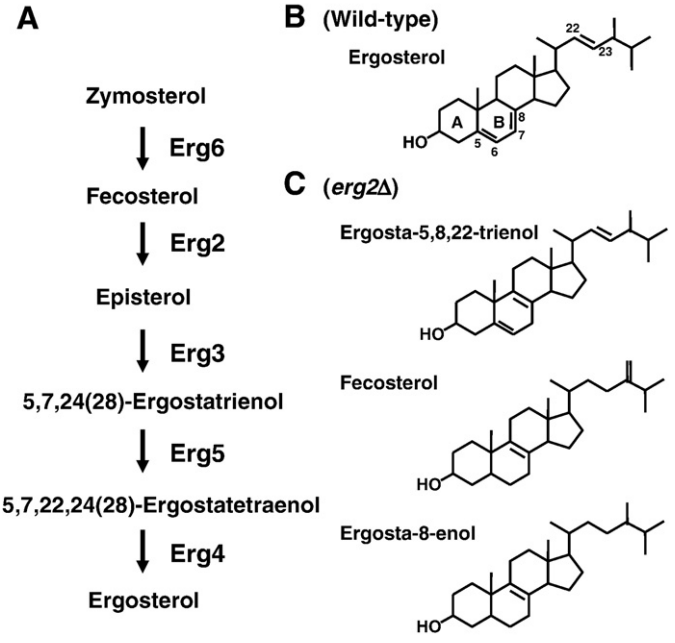


**Fig. 1.** Ergosterol biosynthetic pathway in *S. cerevisiae*. (A) The final five steps in ergosterol biosynthesis. (B) Structure of ergosterol. (C) Structure of altered sterols accumulated in the *erg2*Δ mutant as reported by Heese-Peck et al. [18].

confirmed that rhodamine 6G is highly accumulated in *erg2*Δ and *erg6*Δ mutants under energy-deleted conditions (data not shown).

### 3.2. Rigidity of the plasma membrane analyzed with steady-state and time-resolved fluorescence spectroscopy

To examine whether cycloheximide sensitivity in *erg*Δ mutants was attributable to the loss of rigidity of the plasma membrane, we performed anisotropy measurements on cells labeled with the lipophilic fluorescence probes DPH and TMA-DPH. Cell growth was not compromised with either dye at high concentrations of up to 50 μM in SC medium (data not shown). However, we found that DPH molecules formed aberrant granules predominantly occurring in the cytoplasm rather than localizing to the plasma membrane in the wild-type and *erg2*Δ cells (Fig. 3) even though DPH was used at a low concentration of 0.5 μM (data not shown). The DPH-positive granules are unlikely to be endosomes because FM4-64 [39] did not overlap with the granules, and the granules were still observed when labeling was performed in the presence of $NaN_3$ (data not shown). The DPH-positive granules also occurred in other *erg*Δ mutants (data not shown). To avoid this irrelevance, we did not use DPH for further analyses. In contrast, TMA-DPH clearly localized to the plasma membrane in the cell, and the distribution appeared nearly uniform throughout the plasma membrane (Fig. 3). Due to its cationic moiety, this dye is anchored only in the outer leaflet of the plasma membrane. It was unlikely that internalization of TMA-DPH by endocytosis occurred because the dye still localized only to the plasma membrane even with an extended labeling time of >2 h in growth medium, while FM4-64 accumulated in the vacuole within 30 min of labeling (data not shown). Therefore, TMA-DPH was used for further anisotropy measurements. We found that the fluorescence intensity of TMA-DPH-labeled cells increased with increasing dye concentration, and the trend was more marked in *erg2*Δ, *erg3*Δ, and *erg6*Δ mutants (Fig. 4A). Critically, although the steady-state anisotropy $r_s$ was constant up to the fluorescence intensity of 450 arbitrary units (a.u.), it decreased in highly labeled cells (fluorescence intensity >500 a.u.) (Fig. 4B). To avoid possible artifacts, we fixed the dye concentration in labeling at 0.5 μM to maintain the fluorescence intensity of the labeled cells between 200 to 450 a.u. throughout the study. We found that *erg2*Δ, *erg4*Δ, and *erg6*Δ mutants had lower $r_s$ values compared with the wild-type strain (Table 1). This result is generally consistent with a previous report that examined *erg2*Δ, *erg3*Δ, and *erg6*Δ mutants [35]. However, the degree of steady-state anisotropy cannot give an appropriate

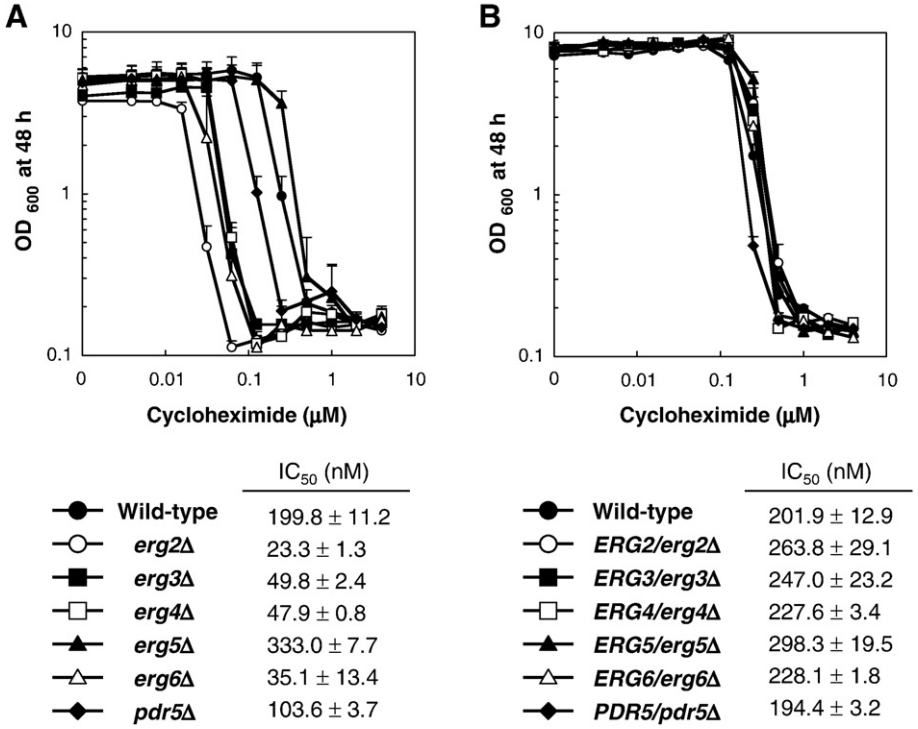


**Fig. 2.** Cycloheximide sensitivity of *erg*Δ mutants. Cells of (A) haploid and (B) heterozygous diploid were cultured in SC medium in the presence of various concentrations of cycloheximide for 48 h. The *erg2*Δ mutant exhibits the most marked hypersensitivity. Data are represented as mean $OD_{600}$ values with standard deviations from three independent experiments.

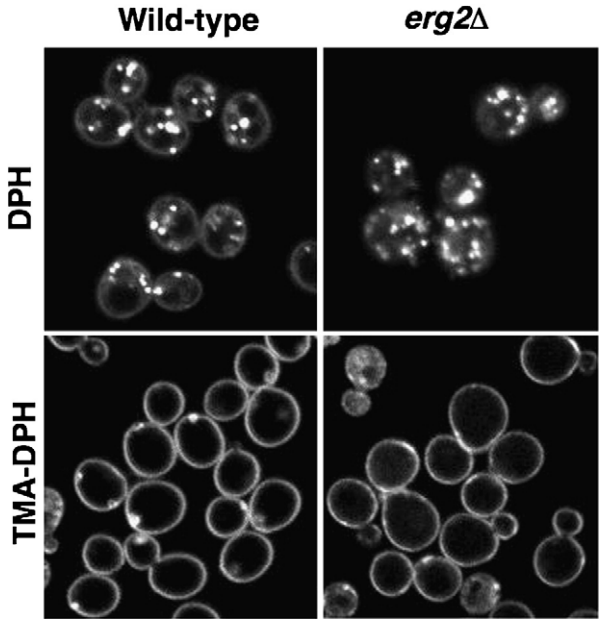


**Fig. 3.** Localization of DPH and TMA-DPH in the cells. Cells of the wild-type strain and *erg2*Δ mutant were labeled with DPH or TMA-DPH in TE buffer for 10 min. The labeled cells were visualized under an FV500 confocal laser microscope. In both strains, DPH formed aberrant granules in the cells, while TMA-DPH localized solely to the plasma membrane.

indication of the cycloheximde sensitivity of the cells because the order of magnitude of $r_s$, *erg6*Δ < *erg4*Δ < *erg2*Δ < *erg5*Δ < *erg3*Δ, wild-type, did not sufficiently correspond to the degree of cycloheximide sensitivity (see below).

To determine the parameters that characterize the rotational motion of TMA-DPH, we performed time-resolved fluorescence spectroscopy. Cells were labeled with TMA-DPH in the same way as for steady-state anisotropy measurement. The DMPC artificial lipid bilayer was used as a reference. It forms a lamellar gel ($L_\beta$'), ripple gel ($P_\beta$'), and liquid crystalline ($L_\alpha$) phase at 10, 20, and 30 °C, respectively. Fig. 5 shows the anisotropic decays of TMA-DPH in the plasma membrane and the DMPC bilayer. Strikingly, we noticed that the yeast plasma membrane was far from fluid but very rigid, analogous to the gel phases of the DMPC bilayer (Fig. 5C, $L_\beta$' and $P_\beta$' phases), and the limiting anisotropy of TMA-DPH $r_\infty$ remained at higher values of around 0.3 in the plasma membrane (Fig. 5A, B) in contrast to a lower $r_\infty$ value of around 0.17 in the $L_\alpha$ phase in the DMPC bilayer (Fig. 5C). This result indicates that the rotational motion of TMA-DPH is highly restricted in the interfacial region of the plasma membrane. The $r_\infty$ value for TMA-DPH in the cells remained almost constant at temperature ranges from 10 to 33 °C, in contrast to the temperature dependency in TMA-DPH in the DMPC bilayer or DPH in the P13 membranes (our unpublished observation). The nonlinear fitting of the decay after convoluting the instrumental response function gave an $r_0$ value of 0.328 ± 0.007, $r_\infty$ value of 0.302 ± 0.006, and rotational correlation time $\theta$ value of 11.3 ± 3.7 ns in the wild-type strain ($n$ = 15), according to Eq. (2) (Table 2). The steady-state anisotropy (Table 1) was expected to be intermediate in value between $r_0$ and $r_\infty$, but it was lower than $r_\infty$ for the unknown reason. We found that deletions for *ERG* genes resulted in very complex changes in parameters that characterized the membrane property (Table 2). Among *erg*Δ mutations, *erg2*Δ exhibited the most remarkable effect on membrane properties. It decreased the $\theta$ value to 2.6 ± 1.9 ns ($n$ = 15), indicating that the rotational motion of TMA-DPH is highly accelerated in the *erg2*Δ membrane. Hence, the rotational diffusion coefficient $D_w$ of TMA-DPH (see Eq. (4)) dramatically increased from 1.3 ± 0.3 (wild-type, $n$ = 15) to 10.6 ± 3.0 $\mu s^{-1}$ (*erg2*Δ, $n$ = 12). The *erg2*Δ mutation resulted in a decrease in the order parameter $S$ of the plasma

**Table 1**
Steady-state anisotropy of TMA-DPH in the wild-type strain and the *erg*Δ mutants[a]

| Genotype | $r_s$[b] | $n$ |
|---|---|---|
| Wild-type | 0.283 ± 0.004 | 5 |
| *erg2*Δ | 0.278 ± 0.003* | 5 |
| *erg3*Δ | 0.283 ± 0.004 | 5 |
| *erg4*Δ | 0.275 ± 0.005* | 5 |
| *erg5*Δ | 0.280 ± 0.007 | 5 |
| *erg6*Δ | 0.272 ± 0.007* | 5 |

$r_s$, steady-state anisotropy; $n$, number of independent experiments.
[a] Measurements were carried out at 25 °C. Data are represented as means ± SD.
[b] Asterisks denote statistical significance with respect to the wild-type strain ($P$<0.05).

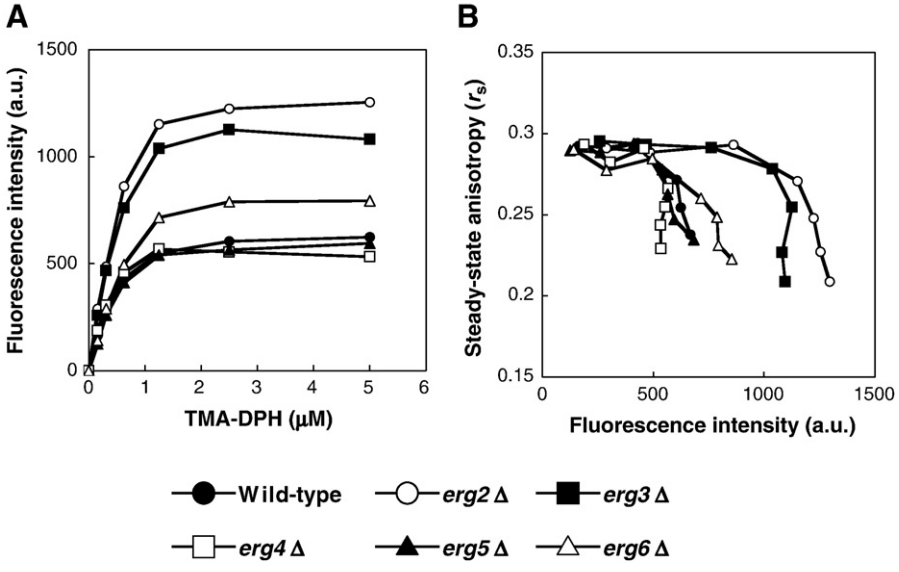


**Fig. 4.** Optimization of cell labeling with TMA-DPH. (A) Cells of the wild-type strain and *erg*Δ mutants were labeled with various concentrations of TMA-DPH in TE buffer. TMA-DPH accumulated abundantly in the *erg2*Δ, *erg3*Δ, and *erg6*Δ plasma membrane. (B) Steady-state anisotropy was almost constant at lower fluorescence intensities in each strain, but significantly decreased at higher intensities. To avoid possible artifacts, we fixed the dye concentration in labeling at 0.5 μM to maintain the fluorescence intensity of the labeled cells between 200 to 450 a.u. throughout the study.

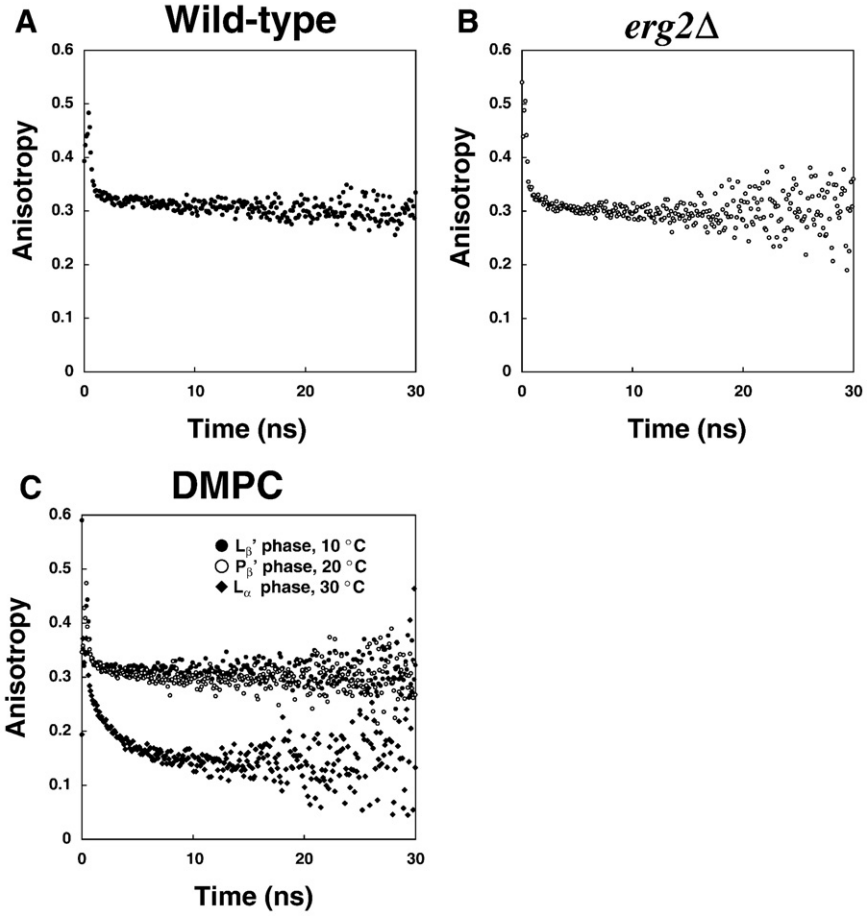


**Fig. 5.** Time-resolved anisotropy measurement of TMA-DPH in the membranes. Cells of the wild-type strain (A) and the *erg2*Δ mutant (B), and 200 μM DMPC lipid bilayer were labeled with 0.5 μM TMA-DPH in TE buffer. The labeled samples were subjected to time-resolved anisotropy measurement at 25 °C (A, B), or at 10, 20, and 30 °C (C) as described in Materials and methods. The parameters characterizing anisotropy decay are presented in Table 2.

membrane, according to Eq. (3), from 0.958±0.006 ($n$=15) to 0.943±0.011 ($n$=12) ($P$<0.005) (Table 2). Analogous to *erg2*Δ, the *erg6*Δ mutation caused an increase in $D_w$ with a decrease in $S$, while the *erg3*Δ mutation increased $D_w$ and $S$, and the *erg4*Δ mutation increased $D_w$ without affecting $S$. The *erg5*Δ mutation had no measurable effect on $D_w$ and $S$. The parameters characterizing the *pdr5*Δ plasma membrane were similar to those of the wild-type strain, which were $r_s$, 0.278±0.002 ($n$=3), $S$, 0.966±0.001 and $D_w$, 1.7±0.3 ($n$=5), suggesting that the reason for the cycloheximide sensitivity of the *pdr5*Δ mutant (Fig. 2) has little relevance to the physicochemical membrane properties. Fig. 6 shows a plot of $D_w$ as a function of $S$ in the wild-type strain and *erg*Δ mutants. There was no marked correlation between $D_w$ and $S$ in the wild-type strain and the *erg*Δ mutants.

It has been demonstrated that $S$ and $D_w$ are important determinants of the diffusion of solutes across the bilayer of 1-palmitoyl-2-oleoyl-*sn*-glycero-3-phosphocholine (POPC). The permeability of mannitol across the POPC membrane increases with decreasing $S$ and increasing $D_w$, and thus permeability depends on the presence and size of voids and the frequency of lipid thermal motion [40]. We considered the possibility of applying this model to explain the cycloheximide permeability of the yeast plasma membrane and hence its toxicity. The 50% growth-inhibitory concentration ($IC_{50}$) of cycloheximide was plotted as a function of $r_s$, $S$, $D_w$, and $S/D_w$. Judging from the correlation factor by exponential approximations of the data, we found that the $IC_{50}$ values were moderately correlated with $S$ and $D_w$ but closely correlated with $S/D_w$ (Fig. 7). This result suggests that decreasing $S$ and increasing $D_w$ synergistically act to enhance drug permeability and result in the sensitivity of *erg*Δ mutants. We assume that altered sterols in the *erg*Δ membranes have low ability to pack the lipid bilayer tightly compared with ergosterol.

In artificial lipid bilayers, membrane rigidity is thought to be influenced not only by the structural motifs of sterols but also by free sterol content in the membrane [41]. Membrane rigidity generally

**Table 2**
Exponential analysis of the anisotropy decay of TMA-DPH in the wild-type strain and the *erg*Δ mutants[a]

| Genotype | $\theta$ (ns) | $r_0$ | $r_\infty$ | $S$[b] | $D_w$ ($\mu s^{-1}$)[b] | $S/D_w$[b] | $\chi^2$ | $n$ |
|---|---|---|---|---|---|---|---|---|
| Wild-type | 11.3±3.7 | 0.328±0.007 | 0.302±0.006 | 0.958±0.006 | 1.3±0.3 | 0.79±0.20 | 1.07±0.05 | 15 |
| *erg2*Δ | 1.8±0.4 | 0.331±0.008 | 0.295±0.010 | 0.943±0.006* | 10.9±3.0* | 0.10±0.03* | 1.10±0.06 | 12 |
| *erg3*Δ | 3.0±1.2 | 0.340±0.007 | 0.319±0.011 | 0.969±0.009* | 3.8±1.7* | 0.30±0.12* | 1.22±0.34 | 8 |
| *erg4*Δ | 8.8±3.4 | 0.327±0.004 | 0.297±0.010 | 0.953±0.007 | 1.9±0.6* | 0.54±0.16* | 1.10±0.05 | 8 |
| *erg5*Δ | 8.3±2.2 | 0.329±0.006 | 0.305±0.010 | 0.962±0.010 | 1.5±0.3 | 0.67±0.16 | 1.08±0.05 | 8 |
| *erg6*Δ | 3.9±1.3 | 0.326±0.009 | 0.292±0.010 | 0.947±0.006* | 4.9±1.6* | 0.22±0.11* | 1.10±0.06 | 11 |

$\theta$; rotational correlation time; $r_0$, maximum anisotropy; $r_\infty$, limiting anisotropy; $S$, order parameter; $D_w$, rotational diffusion coefficient; $n$, number of independent experiments.
[a] Measurements were carried out at 25 °C. Data are represented as means±SD.
[b] Asterisks denote statistical significance with respect to the wild-type strain ($P$<0.005).

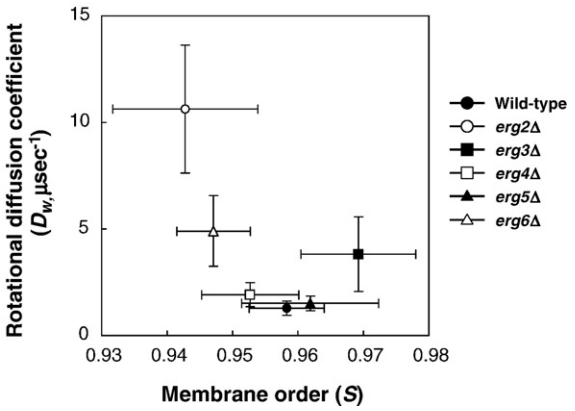


**Fig. 6.** Plot of $D_w$ as a function of $S$ in the wild-type and *erg*Δ strains. Data are from Table 2. There was no marked correlation between $D_w$ and $S$ in the wild-type strain and the *erg*Δ mutants. $D_w$, rotational diffusion coefficient of TMA-DPH; $S$, order parameter for TMA-DPH (see Materials and methods).

increases with increasing sterol content. In our preliminary results with an enzymatic sterol determination (see Materials and methods), the *erg3*Δ and *erg5*Δ mutations increased the free sterol levels 1.4-fold compared with the wild-type strain. In contrast, other *erg* mutations had no significant effect on the sterol levels (data not shown). The increased sterol levels could account for the higher-order parameter of the membranes of the *erg3*Δ and *erg5*Δ mutants (Table 2). Considering the loss of membrane rigidity (Table 2), sterols in *erg2*Δ and *erg6*Δ membranes are insufficient to pack the lipid bilayer tightly due to their specific structural changes. However, we cannot rule out the possibility that the ratio of phosphatidylcholine to phosphatidylethanolamine is altered in *erg2*Δ and *erg6*Δ mutants under our experimental conditions, as reported by Sharma [35], and it may affect the order parameter and the occurrence of voids within the plasma membrane. Precise quantification of sterol and phospholipid contents is required to account for the higher-order parameter of the *erg3*Δ and *erg5*Δ membranes.

### 3.3. Exogenous ergosterol restores the rigidity of the upc2-1erg2Δ plasma membrane

There was a possibility that the *erg*Δ mutation exerted downstream effects such as remodeling in transcription, translation, or cytoskeletal organization, and these effects might cause marked changes in membrane properties. To verify the significance of the role of ergosterol in membrane integrity and dynamics, we examined whether the exogenous addition of ergosterol restored the membrane properties of the *erg*Δ mutant with respect to membrane rigidity. Cells under aerobic conditions do not take up substantial amounts of ergosterol from the medium. A specific mutation, *upc2-1*, allows aerobically growing cells to take up exogenous ergosterol [37,42]. Because of its significance, we only focused on the *erg2*Δ mutation. The *upc2-1erg2*Δ mutant was created to investigate the effects of exogenous ergosterol on membrane properties. Cells of the *upc2-1* and *upc2-1erg2*Δ mutants were

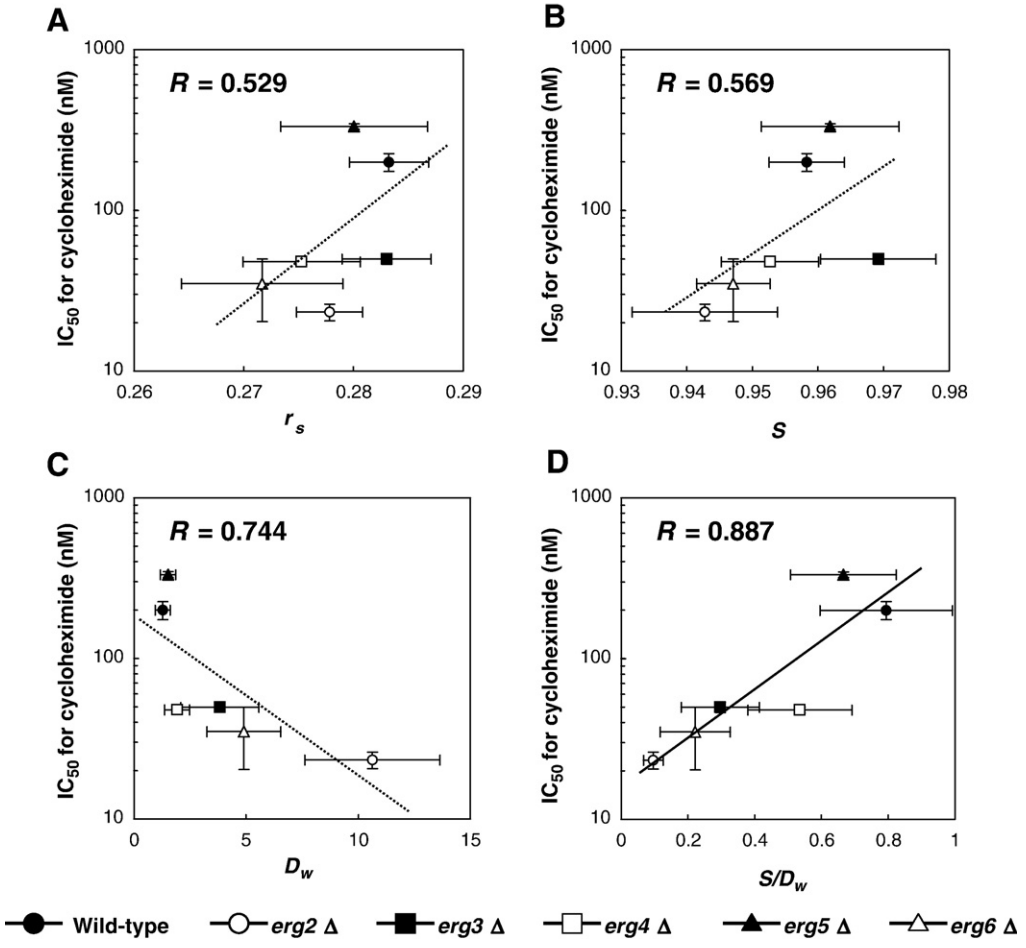


**Fig. 7.** Correlations of parameters describing the membrane properties and $IC_{50}$ values for cycloheximide in the wild-type and *erg*Δ strains. Data are from Fig. 2, Tables 1, and 2. There is a clear correlation between $S/D_w$ and minimum inhibitory concentration. $r_s$, steady-state anisotropy; $D_w$, rotational diffusion coefficient of TMA-DPH; $S$, order parameter for TMA-DPH (see Materials and methods).

**Table 3**
Effects of exogeneous ergosterol on the anisotropy decay of TMA-DPH in the *upc2-1* strain and *upc2-1erg2*Δ mutant[a]

| Genotype | $\theta$ (ns) | $r_0$ | $r_\infty$ | $S$[b] | $D_w$ ($\mu s^{-1}$)[b] | $S/D_w$[b] | $\chi^2$ | $n$ |
|---|---|---|---|---|---|---|---|---|
| *upc2-1* (+ vehicle alone) | 7.8±0.9 | 0.325±0.005 | 0.302±0.006 | 0.963±0.004 | 1.6±0.08 | 0.62±0.03 | 1.07±0.04 | 5 |
| *upc2-1* (+50 μM ergosterol) | 9.2±2.0 | 0.326±0.007 | 0.302±0.010 | 0.962±0.006 | 1.4±0.4 | 0.72±0.17 | 1.13±0.04 | 5 |
| *upc2-1* (+500 μM ergosterol) | 9.6±0.5 | 0.328±0.006 | 0.304±0.008 | 0.962±0.003 | 1.3±0.1*** | 0.74±0.06*** | 1.11±0.03 | 5 |
| *upc2-1erg2*Δ (+ vehicle alone) | 1.3±0.8 | 0.335±0.013 | 0.302±0.015 | 0.949±0.011 | 15.4±7.4 | 0.08±0.06 | 1.14±0.08 | 4 |
| *upc2-1erg2*Δ (+50 μM ergosterol) | 5.2±1.8 | 0.331±0.011 | 0.306±0.014 | 0.961±0.007* | 2.8±1.3*** | 0.40±0.16*** | 1.10±0.03 | 4 |
| *upc2-1erg2*Δ (+500 μM ergosterol) | 5.5±3.1 | 0.332±0.010 | 0.306±0.012 | 0.960±0.006** | 2.9±1.3*** | 0.41±0.25*** | 1.07±0.02 | 4 |

$\theta$; rotational correlation time; $r_0$, maximum anisotropy; $r_\infty$, limiting anisotropy; $S$, order parameter; $D_w$, rotational diffusion coefficient; $n$, number of independent experiments.
[a] Measurements were carried out at 25 °C. Data are represented as means±SD.
[b] Asterisks denote statistical significance with respect to the wild-type strain (*, $P<0.2$; **, $P<0.1$; ***, $P<0.05$).

incubated overnight in the presence of 50 or 500 μM ergosterol. Under these conditions, the cells contain a mix of ergosterol and altered sterols. Subsequently, the cells were labeled with TMA-DPH in the absence of ergosterol. In the *upc2-1* strain, exogenous ergosterol at concentrations of both 50 and 500 μM did not measurably affect the order parameter $S$ and the rotational diffusion coefficient $D_w$, suggesting that the sterol content had been optimized in the wild-type plasma membrane (Table 3). Notably, exogenous ergosterol substantially restored the rigidity of the plasma membrane in the *upc2-1erg2*Δ mutant judging from the increase in $S$ from 0.949±0.011 (vehicle alone) to 0.961±0.007 (50 μM ergosterol) ($P<0.2$), and the decrease in $D_w$ from 15.4±7.4 $\mu s^{-1}$ (vehicle alone) to 2.8±1.3 $\mu s^{-1}$ (50 μM ergosterol) ($P<0.05$) (Table 3). We conclude that exogenous ergosterol fills voids within the *erg2*Δ plasma membrane and that the specific structural motif of ergosterol but not downstream effectors is a major determinant of the rigidity of the plasma membrane. We next examined whether exogenous ergosterol restores the growth defect of the *upc2-1erg2*Δ mutant. Cells of the *upc2-1* and *upc2-1erg2*Δ mutants were grown on SC plates in the presence of cycloheximide and 50 μM ergosterol for 3 days. In support of our hypothesis, exogenous ergosterol restored the growth of the *upc2-1erg2*Δ cells in the presence of 31 to 125 μM cycloheximide (Fig. 8).

## 4. Discussion

In this study, we focused on the role of ergosterol in the integrity and dynamics of the yeast plasma membrane by comparing parameters characterizing membrane properties between the wild-type strain and *erg*Δ mutants. The main findings were: (i) The interfacial region of the plasma membrane is highly rigid, analogous to the gel phase of the DMPC bilayer. (ii) The sterol alteration in the *erg*Δ mutants, particularly in *erg2*Δ, compromises the rigidity of the interfacial region of the plasma membrane, leading to enhanced rotational motion of TMA-DPH. (iii) The altered sterols are likely to fail to pack lipid acyl chains and thereby create voids within the plasma membrane.

It has been demonstrated that $S$ and $D_w$ are important determinants of the diffusion of solutes across the POPC bilayer and that permeability depends on the presence and size of voids and the frequency of lipid thermal motion [40]. Given the permeability of drugs across the yeast plasma membrane, our present results showing decreasing $S$ and increasing $D_w$ values are relevant to the hypersensitivity to cychloheximide of *erg*Δ mutants (Fig. 7D). Thus, our findings highlight the importance of membrane thermodynamics in investigations of environmental responses in yeast physiology. The maximum

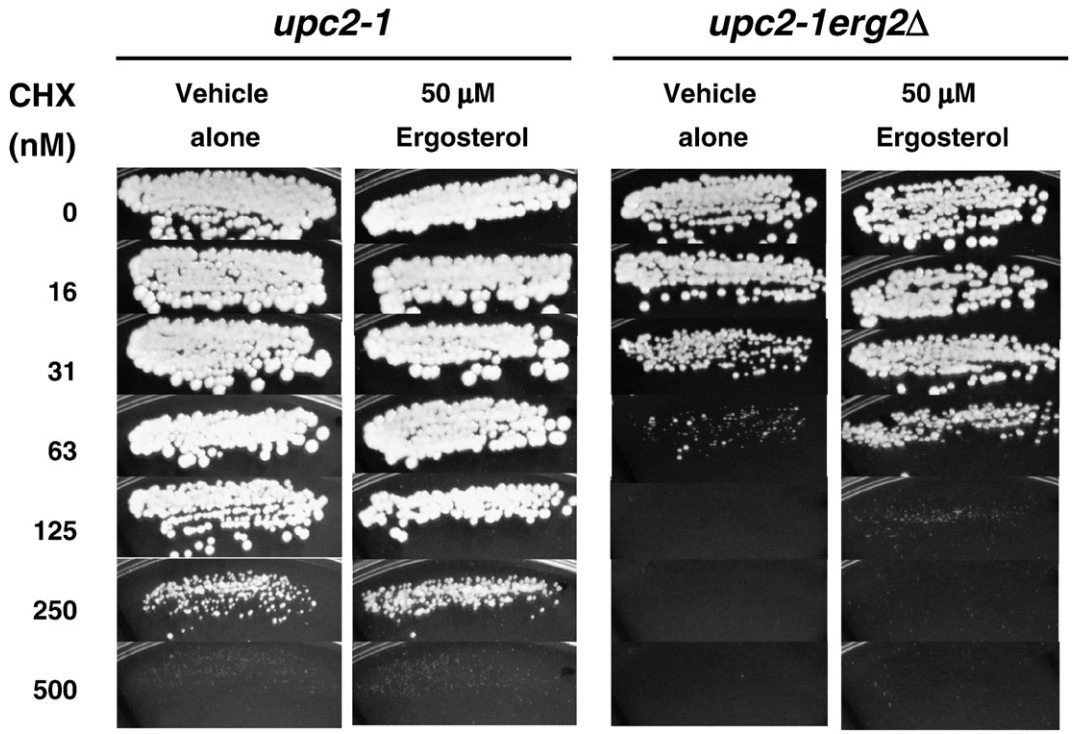


**Fig. 8.** Exogenous ergosterol restores growth defects in *upc2-1erg2*Δ mutants. Cells of the *upc2-1* and *upc2-1erg2*Δ mutants were grown on SC plates in the presence of cycloheximide and 50 μM ergosterol for 3 days. CHX, cycloheximide.

anisotropy of TMA-DPH derived in this study ($r_0$ = 0.328–0.330) (Table 2) was close to that obtained in the bovine adrenal cortex ($r_0$ = 0.320) [43] but lower than the theoretical value of 0.39 [27]. It is assumed that this is partly because the absorption and emission of a TMA-DPH molecule are not parallel [34], but mainly because it is very difficult to derive $r_0$ with a single exponential approximation of the initial time derivative of the rapid anisotropy decay in the case of natural membranes. In our calculation, a two-component exponential approximation yielded a mean $r_0$ value close to 0.39, but the value varied significantly with the experiment and was, for example, 0.381 ± 0.033 ($n$ = 14) and 0.371 ± 0.021 ($n$ = 14) in the wild-type strain and *erg2*Δ mutant, respectively. Therefore, we adopted the single exponential approximation in this study. In any case, the marked increase in the rotational diffusion coefficient elicited by the *erg2*Δ mutation is evident.

The altered sterols in the *erg2*Δ mutant are in some ways structurally similar to cholesterol rather than to ergosterol with respect to the lack of the C-7,8 and C-22,23 double bonds (Fig. 1B). A molecular dynamic study indicated that the tilt angles of the sterol ring system and sterol side chains are greater in cholesterol than in ergosterol [44]. Consequently, cholesterol has less packing efficiency of lipid acyl chains than ergosterol in lipid bilayers. Electron density profiles of the simulated systems along the bilayer normally indicate that the thickness of DMPC bilayer containing 25 mol% of ergosterol is higher than that containing the same amount of cholesterol, and hence ergosterol has greater ability to stiffen the bilayer than cholesterol [44]. Such steric hindrance is assumed to interfere with hydrogen bonding between lipid molecules within the *erg2*Δ plasma membrane, leading to reduced membrane order. It has been demonstrated that the side-chain methylation by Δ24 methyltransferase (Erg6) as well as appropriate B-ring desaturation in ergosterol is required for efficient ligand-induced Ste2 internalization [18]. Our finding indicates that the *erg6*Δ mutation diminished the rigidity of the membrane less than the *erg2*Δ mutation. In the *erg6*Δ mutant, the plasma membrane is known to be enriched in equivalent amounts of zymosterol and cholesta-5,7,24-trienol [18]. Cholesta-5,7,24-trienol but not zymosterol has a C-7,8 double bond. Thus, half of the sterols with the C-7,8 double bond in the *erg6*Δ mutant likely contribute to moderate packing of the plasma membrane. Altered sterols in the *erg3*Δ mutant are also different from ergosterol with respect to the lack of the C-5,6 but not the C-7,8 double bond. However, the mutant is more resistant to cycloheximide than the *erg2*Δ mutant. It is possible that an increased amount of sterols compensates for the defect in membrane rigidity in the *erg3*Δ mutant affecting $S$ and $D_w$ (Table 2). In this respect, the hyperresistance to cycloheximide of the *erg5*Δ mutant could also be accounted for by an increased amount of altered sterols. It remains unknown whether specific structural motifs or the overall structure of the ergosterol molecule is a prerequisite for the bulk membrane properties.

A primarily important question to be answered is why the *erg* mutants exhibit pleiotropic hypersensitivity. We have confirmed that the *erg* mutants, particularly *erg2*Δ, exhibit pleiotropic hypersensitivity to some compounds such as LiCl, NaCl, and ethanol (unpublished observation). No matter how the *erg2*Δ membrane loses its rigidity, it is unlikely to occur that passive influx of $Li^+$ and $Na^+$ is enhanced across the lipid moiety of *erg2*Δ plasma membrane. Alternatively, it is more likely that incorporation of the cations through ion channels is excessive in the *erg2*Δ mutant. Considering the high hydration force of the alkali cations, we speculate that bound water molecules that stabilize the structure of membrane proteins could be extracted when $Li^+$ and $Na^+$ are abundant. Because the *erg2*Δ plasma membrane loses its rigidity (Table 2), this situation is likely to become more prominent in the *erg2*Δ mutant. Upon extraction of bound water, ion channels might be destabilized allowing excessive incorporation of $Li^+$ and $Na^+$ into the cytoplasm.

Ergosterol has more pronounced effects on domain formation in the sphingomyelin/DPPC model membrane than cholesterol according to a study using fluorescence-quenching and detergent-insolubility methods [45]. We are in the process of investigating the role of sphingolipids in membrane dynamics in coordination with ergosterol using time-resolved fluorescence spectroscopy. Membrane proteins are surrounded by a shell of lipid molecules. The surface of a membrane protein contains shallow grooves and protrusions to which fatty acids and sterols conform to provide tight packing and function (reviewed in [46,47]). Altered sterols in *erg*Δ mutants might be deficient in the packing of some plasma membrane proteins, which have conformed to ergosterol for optimal functions. Macroscopic segregation of Pma1 and the arginine permease Can1 was observed in the plasma membrane [48]. Investigations are required to verify the relevance of the lateral segregation of lipid molecules and the physicochemical properties of membrane domains, and the association of the proteins with DRMs. Our findings provide mechanical insights into the role of ergosterol in a variety of cellular processes such as endocytosis and membrane trafficking as well as bulk membrane functions.

## Acknowledgements

We thank Keiko Usui for technical support; William A. Prinz for proving yeast strains; Yuichi Nogi, Hiroki Baba, Kulwinder Sagoo, and Ayako Kikuchi for technical suggestions; Hisashi Uedaira, Saame R. Shaikh and Michael Edidin for critical reading of this manuscript; and Roland Winter, Hiroaki Minegishi, Yoichi Noda, Koji Yoda, Hitoshi Matsuki, Shoji Kaneshina, and Koki Horikoshi for valuable comments and discussions. This work was supported by the Japan Society for the Promotion of Science (No. 18658039 to F. Abe).

## References

[1] M.J. Karnovsky, A.M. Kleinfeld, R.L. Hoover, R.D. Klausner, The concept of lipid domains in membranes, J. Cell. Biol. 94 (1982) 1–6.
[2] K. Simons, E. Ikonen, Functional rafts in cell membranes, Nature 387 (1997) 569–572.
[3] M. Edidin, The state of lipid rafts: from model membranes to cells, Annu. Rev. Biophys. Biomol. Struct. 32 (2003) 257–283.
[4] J.A. Allen, R.A. Halverson-Tamboli, M.M. Rasenick, Lipid raft microdomains and neurotransmitter signalling, Nat. Rev. Neurosci. 8 (2007) 128–140.
[5] V. Michel, M. Bakovic, Lipid rafts in health and disease, Biol. Cell 99 (2007) 129–140.
[6] M. Bagnat, S. Keranen, A. Shevchenko, A. Shevchenko, K. Simons, Lipid rafts function in biosynthetic delivery of proteins to the cell surface in yeast, Proc. Natl. Acad. Sci. U. S. A. 97 (2000) 3254–3259.
[7] L.W. Parks, W.M. Casey, Physiological implications of sterol biosynthesis in yeast, Annu. Rev. Microbiol. 49 (1995) 95–116.
[8] M.A. Ghannoum, L.B. Rice, Antifungal agents: mode of action, mechanisms of resistance, and correlation of these mechanisms with bacterial resistance, Clin. Microbiol. Rev. 12 (1999) 501–517.
[9] N.D. Lees, B. Skaggs, D.R. Kirsch, M. Bard, Cloning of the late genes in the ergosterol biosynthetic pathway of *Saccharomyces cerevisiae* —a review, Lipids 30 (1995) 221–226.
[10] L.W. Parks, J.H. Crowley, F.W. Leak, S.J. Smith, M.E. Tomeo, Use of sterol mutants as probes for sterol functions in the yeast, *Saccharomyces cerevisiae*, Crit. Rev. Biochem. Mol. Biol. 34 (1999) 399–404.
[11] C. Novotny, M. Flieger, J. Panos, F. Karst, Effect of 5,7-unsaturated sterols on ethanol tolerance in *Saccharomyces cerevisiae*, Biotechnol. Appl. Biochem. 15 (1992) 314–320.
[12] J.P. Vogel, J.N. Lee, D.R. Kirsch, M.D. Rose, E.S. Sztul, Brefeldin A causes a defect in secretion in *Saccharomyces cerevisiae*, J. Biol. Chem. 268 (1993) 3040–3043.
[13] A.A. Welihinda, A.D. Beavis, R.J. Trumbly, Mutations in *LIS1* (*ERG6*) gene confer increased sodium and lithium uptake in *Saccharomyces cerevisiae*, Biochim. Biophys. Acta 1193 (1994) 107–117.
[14] T. Inoue, H. Iefuji, T. Fujii, H. Soga, K. Satoh, Cloning and characterization of a gene complementing the mutation of an ethanol-sensitive mutant of sake yeast, Biosci. Biotechnol. Biochem. 64 (2000) 229–236.
[15] R. Emter, A. Heese-Peck, A. Kralli, *ERG6* and *PDR5* regulate small lipophilic drug accumulation in yeast cells via distinct mechanisms, FEBS Lett. 521 (2002) 57–61.
[16] R. Kaur, A.K. Bachhawat, The yeast multidrug resistance pump, Pdr5p, confers reduced drug resistance in erg mutants of *Saccharomyces cerevisiae*, Microbiology 145 (Pt 4) (1999) 809–818.
[17] A.L. Munn, A. Heese-Peck, B.J. Stevenson, H. Pichler, H. Riezman, Specific sterols required for the internalization step of endocytosis in yeast, Mol. Biol. Cell 10 (1999) 3943–3957.

[18] A. Heese-Peck, H. Pichler, B. Zanolari, R. Watanabe, G. Daum, H. Riezman, Multiple functions of sterols in yeast endocytosis, Mol. Biol. Cell 13 (2002) 2664–2680.
[19] T. Iwaki, H. Iefuji, Y. Hiraga, A. Hosomi, T. Morita, Y. Giga-Hama, K. Takegawa, Multiple functions of ergosterol in the fission yeast *Schizosaccharomyces pombe*, Microbiology 154 (2008) 830–841.
[20] K. Umebayashi, A. Nakano, Ergosterol is required for targeting of tryptophan permease to the yeast plasma membrane, J. Cell Biol. 161 (2003) 1117–1131.
[21] K. Daicho, H. Maruyama, A. Suzuki, M. Ueno, M. Uritani, T. Ushimaru, The ergosterol biosynthesis inhibitor zaragozic acid promotes vacuolar degradation of the tryptophan permease Tat2p in yeast, Biochim. Biophys. Acta 1768 (2007) 1681–1690.
[22] M. Eisenkolb, C. Zenzmaier, E. Leitner, R. Schneiter, A specific structural requirement for ergosterol in long-chain fatty acid synthesis mutants important for maintaining raft domains in yeast, Mol. Biol. Cell 13 (2002) 4414–4428.
[23] T. Kishimoto, T. Yamamoto, K. Tanaka, Defects in structural integrity of ergosterol and the Cdc50p-Drs2p putative phospholipid translocase cause accumulation of endocytic membranes, onto which actin patches are assembled in yeast, Mol. Biol. Cell 16 (2005) 5592–5609.
[24] H. Jin, J.M. McCaffery, E. Grote, Ergosterol promotes pheromone signaling and plasma membrane fusion in mating yeast, J. Cell Biol. 180 (2008) 813–826.
[25] F. Abe, H. Minegishi, Global screening of genes essential for growth in high-pressure and cold environments: searching for basic adaptive strategies using a yeast deletion library, Genetics 178 (2008) 851–872.
[26] K. Kinosita Jr, S. Kawato, A. Ikegami, A theory of fluorescence polarization decay in membranes, Biophys. J. 20 (1977) 289–305.
[27] F.G. Prendergast, R.P. Haugland, P.J. Callahan, 1-[4-(Trimethylamino)phenyl]-6-phenylhexa-1,3,5-triene: synthesis, fluorescence properties, and use as a fluorescence probe of lipid bilayers, Biochemistry 20 (1981) 7333–7338.
[28] B.R. Lentz, Use of fluorescent probes to monitor molecular order and motions within liposome bilayers, Chem. Phys. Lipids 64 (1993) 99–116.
[29] B.R. Lentz, Y. Barenholz, T.E. Thompson, Fluorescence depolarization studies of phase transitions and fluidity in phospholipid bilayers. 2 Two-component phosphatidylcholine liposomes, Biochemistry 15 (1976) 4529–4537.
[30] B. Cannon, G. Heath, J. Huang, P. Somerharju, J.A. Virtanen, K.H. Cheng, Time-resolved fluorescence and Fourier transform infrared spectroscopic investigations of lateral packing defects and superlattice domains in compositionally uniform cholesterol/phosphatidylcholine bilayers, Biophys. J. 84 (2003) 3777–3791.
[31] S. Shrivastava, A. Chattopadhyay, Influence of cholesterol and ergosterol on membrane dynamics using different fluorescent reporter probes, Biochem. Biophys. Res. Commun. 356 (2007) 705–710.
[32] J.G. Kuhry, P. Fonteneau, G. Duportail, C. Maechling, G. Laustriat, TMA-DPH: a suitable fluorescence polarization probe for specific plasma membrane fluidity studies in intact living cells, Cell Biophys. 5 (1983) 129–140.
[33] C. Low, R.J. Rodriguez, L.W. Parks, Modulation of yeast plasma membrane composition of a yeast sterol auxotroph as a function of exogenous sterol, Arch. Biochem. Biophys. 240 (1985) 530–538.
[34] H. van Langen, G. van Ginkel, D. Shaw, Y.K. Levine, The fidelity of response by 1-[4-(trimethylammonio)phenyl]-6-phenyl-1,3,5-hexatriene in time-resolved fluorescence anisotropy measurements on lipid vesicles. Effects of unsaturation, headgroup and cholesterol on orientational order and reorientational dynamics, Eur. Biophys. J. 17 (1989) 37–48.
[35] S.C. Sharma, Implications of sterol structure for membrane lipid composition, fluidity and phospholipid asymmetry in *Saccharomyces cerevisiae*, FEMS Yeast Res. 6 (2006) 1047–1051.
[36] G. Giaever, A.M. Chu, L. Ni, C. Connelly, L. Riles, S. Veronneau, S. Dow, A. Lucau-Danila, K. Anderson, B. Andre, A.P. Arkin, A. Astromoff, M. El-Bakkoury, R. Bangham, R. Benito, S. Brachat, S. Campanaro, M. Curtiss, K. Davis, A. Deutschbauer, K.D. Entian, P. Flaherty, F. Foury, D.J. Garfinkel, M. Gerstein, D. Gotte, U. Guldener, J.H. Hegemann, S. Hempel, Z. Herman, D.F. Jaramillo, D.E. Kelly, S.L. Kelly, P. Kotter, D. LaBonte, D.C. Lamb, N. Lan, H. Liang, H. Liao, L. Liu, C. Luo, M. Lussier, R. Mao, P. Menard, S.L. Ooi, J.L. Revuelta, C.J. Roberts, M. Rose, P. Ross-Macdonald, B. Scherens, G. Schimmack, B. Shafer, D.D. Shoemaker, S. Sookhai-Mahadeo, R.K. Storms, J.N. Strathern, G. Valle, M. Voet, G. Volckaert, C.Y. Wang, T.R. Ward, J. Wilhelmy, E.A. Winzeler, Y. Yang, G. Yen, E. Youngman, K. Yu, H. Bussey, J.D. Boeke, M. Snyder, P. Philippsen, R.W. Davis, M. Johnston, Functional profiling of the *Saccharomyces cerevisiae* genome, Nature 418 (2002) 387–391.
[37] Y. Li, W.A. Prinz, ATP-binding cassette (ABC) transporters mediate nonvesicular, raft-modulated sterol movement from the plasma membrane to the endoplasmic reticulum, J. Biol. Chem. 279 (2004) 45226–45234.
[38] F. Abe, H. Iida, Pressure-induced differential regulation of the two tryptophan permeases Tat1 and Tat2 by ubiquitin ligase Rsp5 and its binding proteins, Bul1 and Bul2, Mol. Cell. Biol. 23 (2003) 7566–7584.
[39] T.A. Vida, S.D. Emr, A new vital stain for visualizing vacuolar membrane dynamics and endocytosis in yeast, J. Cell Biol. 128 (1995) 779–792.
[40] M. Sutter, T. Fiechter, G. Imanidis, Correlation of membrane order and dynamics derived from time-resolved fluorescence measurements with solute permeability, J. Pharm. Sci. 93 (2004) 2090–2107.
[41] C. Bernsdorff, A. Wolf, R. Winter, E. Gratton, Effect of hydrostatic pressure on water penetration and rotational dynamics in phospholipid-cholesterol bilayers, Biophys. J. 72 (1997) 1264–1277.
[42] J.H. Crowley, F.W. Leak Jr, K.V. Shianna, S. Tove, L.W. Parks, A mutation in a purported regulatory gene affects control of sterol uptake in *Saccharomyces cerevisiae*, J. Bacteriol. 180 (1998) 4177–4183.
[43] B. de Foresta, M. Rogard, M. le Maire, J. Gallay, Effects of temperature and benzyl alcohol on the structure and adenylate cyclase activity of plasma membranes from bovine adrenal cortex, Biochim. Biophys. Acta 905 (1987) 240–256.
[44] G. M'baye, Y. Mely, G. Duportail, A.S. Klymchenko, Liquid ordered and gel phases of lipid bilayers: fluorescent probes reveal close fluidity but different hydration, Biophys. J. 95 (2008) 1217–1225.
[45] X. Xu, R. Bittman, G. Duportail, D. Heissler, C. Vilcheze, E. London, Effect of the structure of natural sterols and sphingolipids on the formation of ordered sphingolipid/sterol domains (rafts). Comparison of cholesterol to plant, fungal, and disease-associated sterols and comparison of sphingomyelin, cerebrosides, and ceramide, J. Biol. Chem. 276 (2001) 33540–33546.
[46] A.G. Lee, Lipid–protein interactions in biological membranes: a structural perspective, Biochim. Biophys. Acta 1612 (2003) 1–40.
[47] R.M. Epand, Cholesterol and the interaction of proteins with membrane domains, Prog. Lipid Res. 45 (2006) 279–294.
[48] K. Malinska, J. Malinsky, M. Opekarova, W. Tanner, Visualization of protein compartmentation within the plasma membrane of living yeast cells, Mol. Biol. Cell 14 (2003) 4427–4436.